

Manganese-doped $(1 - x)\text{BiScO}_3-x\text{PbTiO}_3$ high-temperature ferroelectrics: Defect structure and mechanism of enhanced electric resistivity

Michael D. Drahus,¹ Peter Jakes,¹ Emre Erdem,¹ Silke Schaab,² Jun Chen,² Mykhaylo Ozerov,³ Sergei Zvyagin,³ and Rüdiger-A. Eichel^{1,*}

¹*Institut für Physikalische Chemie I, Universität Freiburg, Albertstraße 21, D-79104 Freiburg, Germany*

²*NAW, Technische Universität Darmstadt, D-64287 Darmstadt, Germany*

³*Dresden High Magnetic Field Laboratory (HLD), Helmholtz-Zentrum Dresden-Rossendorf, D-01314 Dresden, Germany*

(Received 5 October 2010; revised manuscript received 11 April 2011; published 23 August 2011)

The effect of multivalency manganese doping on the defect structure and enhanced electrical resistivity is studied for the high-temperature piezoelectric $(1 - x)\text{BiScO}_3-x\text{PbTiO}_3$ (BSPT) solid-solution system by means of multifrequency electron paramagnetic resonance spectroscopy combined with conductivity measurements. The results show that manganese is rather incorporated on a scandium than a titanium site as an isovalent substitute ($\text{Mn}_{\text{Sc}}^{\times}$) instead of acceptor-type centers, such as $\text{Mn}_{\text{Ti}}^{\prime}$, $\text{Mn}_{\text{Ti}}^{\prime\prime}$, or $\text{Mn}_{\text{Sc}}^{\bullet}$. The enhanced electric resistivity is found being on the one hand due to the trapping of conduction electrons at the manganese functional center sites ($\text{Mn}_{\text{Sc}}^{\times} + e' \rightarrow \text{Mn}_{\text{Sc}}^{\bullet}$). On the other hand, through the formation of $(\text{Mn}_{\text{Sc}}^{\bullet} - V_{\text{O}}^{\bullet\bullet})^{\bullet}$ defect complexes the ionic conductivity is reduced. Concerning the overall mechanism of charge compensation in that material, both kinds of defects mutually compensate.

DOI: 10.1103/PhysRevB.84.064113

PACS number(s): 61.72.J-, 61.72.Bb, 85.50.-n

I. INTRODUCTION

A promising material for high-temperature piezoelectric actuator and transducer applications¹ is the $(1 - x)\text{BiScO}_3-x\text{PbTiO}_3$ (BSPT) solid-solution system^{2,3} owing to the considerably higher Curie temperature T_C for the ferroelectric-paraelectric transition as compared to conventional piezoelectrics, such as lead zirconate titanate (PZT).⁴ Like PZT, the best piezoelectric activity is found near the morphotropic phase boundary (MPB) between the tetragonal and rhombohedral phase.⁵⁻⁸ State-of-the-art modified BSPT compounds with a composition at the morphotropic phase boundary ($x = 0.64$) exhibit Curie temperatures of $T_C > 400$ °C,⁹ as compared to $T_C \approx 360$ °C for “soft” PZT 52/48.

A major drawback for high-temperature piezoelectric devices is the fact that polycrystalline ferroelectric materials often are extrinsic semiconductors owing to impurities and charged defects. As a consequence they possess an inherently high level of conductivity at elevated temperatures.¹⁰ A strategy to circumvent this problem is the doping with multivalent manganese, such as has been reported recently for various Bi-containing high-temperature piezoelectrics, such as $\text{CaBi}_4\text{Ti}_4\text{O}_{15}$,¹¹ $(1 - x)\text{BiFeO}_3-x\text{BaTiO}_3$ (BFBT),¹² and BSPT.⁹ An alternative strategy to circumvent the problem of electrical conductivity is the application of an uniaxial mechanical load.¹³

With respect to electrical conductivity, two different mechanisms of conductivity have to be distinguished—*electronic* conductivity through conduction electrons or holes (e' , h^{\bullet}) and *ionic* conductivity through the drift-diffusion of oxygen vacancies ($V_{\text{O}}^{\bullet\bullet}$). A means to investigate the interplay between the manganese functional centers and both kind of conduction mechanisms is provided by electron paramagnetic resonance (EPR) spectroscopy.^{14,15}

Concerning the defect structure, it is not possible to simply transfer the principles of defect chemistry established for PZT^{14,15} to Bi-containing piezoelectrics.¹⁶ Whereas in PZT the perovskite A site is divalent (Pb^{2+}) and the B site is

tetravalent (Zr^{4+} , Ti^{4+}), in BSPT the A and B sites are mixed di- and trivalent (Pb^{2+} , Sc^{3+}) and mixed tri- and tetravalent (Sc^{3+} , Ti^{4+}), respectively. Therefore, manganese functional centers incorporated on the B site may be incorporated either as isovalent substitution $\text{Mn}_{\text{Sc}}^{\times}$ ($\text{Mn}_{\text{Ti}}^{\times}$) or as aliovalent acceptor (donor) type $\text{Mn}_{\text{Ti}}^{\prime}$ ($\text{Mn}_{\text{Sc}}^{\bullet}$) ions depending on their oxidation state.

II. EXPERIMENTAL

0.5 mol % manganese-doped $(1 - x)\text{BiScO}_3-x\text{PbTiO}_3$ ceramics ($x = 0.60, 0.62, 0.64, \text{ and } 0.66$) were prepared by the conventional solid-state reaction method.² The precursors of PbO (99.9%, Alfa Aesar), TiO_2 (99.9%, Alfa Aesar), MnO_2 (99.9%, Alfa Aesar), Bi_2O_3 (99.975%, Alfa Aesar), and Sc_2O_3 (99.9%, Alfa Aesar) were mixed according to the stoichiometric formulas of each composition. The mixture of precursors was ball milled in ethanol for 12 h. The dried powders were calcined at 760 °C for 5 h and ball milled again for 12 h. Calcined powders were uniaxially pressed into pellets with a diameter of 10 mm and thickness of ≈ 1.0 mm, and then compacted at 200 MPa by cold isostatic pressure (CIP). The green compacts were embedded in the calcined powders of the same composition and sintered in a covered crucible at 1100 °C for 1 h.

Further heat treatment under controlled atmosphere conditions was carried out in a tube furnace at 1000 °C for 3 h under the flowing gas of the following atmospheres: O_2 (99.8%) and H_2 (99.95%). At the end of the heat treating time the furnace was shut off and allowed to cool to room temperature.

For electric measurements the samples were ground down to a thickness of approximately 300 μm , polished, and annealed before platinum electrodes were sputtered. A triangular wave form at a frequency of 100 mHz was applied to detect field-induced polarization (P) and longitudinal strain (S) curves in a silicone oil bath by using a Sawyer-Tower circuit equipped with an optical sensor. Electrical resistivity was

measured on hot-poled, field-cooled samples (1.8 kV/mm at 200 °C for 5 min) using the Keithley 6517B electrometer. Data were taken by applying a voltage of about 60 V (200 V/mm) above the Curie temperature.

The X-band (9.4 GHz) EPR measurements were performed on a Bruker ESP 380 spectrometer with an H_{011} cavity at ambient temperature. The high-frequency (104 and 208 GHz) EPR spectra were obtained using a tunable frequency EPR spectrometer similar to that described in Ref. 17 at the Dresden High Magnetic Field Laboratory.

III. THEORY

For a theoretical description of the obtained EPR spectra, the spin-Hamiltonian concept is used.¹⁸ The free di-, tri-, and tetravalent manganese ions have electronic configurations between $3d^5$ and $3d^3$ with ground-state electron spins of $S = \frac{5}{2}, 2, \frac{3}{2}$, respectively. The corresponding spin Hamiltonian can then be written as

$$\mathcal{H} = \beta_e \mathbf{B}_0 \cdot \mathbf{g} \cdot \mathbf{S} + \sum_{k=2, \dots, 2S}^{-k \leq q \leq k} B_k^q O_k^q(S_x, S_y, S_z) + \mathbf{S} \cdot {}^{55}\mathbf{A} \cdot \mathbf{I}, \quad (1)$$

where β_e denotes the Bohr magneton, \mathbf{B}_0 is the external magnetic field, \mathbf{g} is the electron g matrix, B_k^q are the fine-structure (FS) Hamiltonian coefficients, and O_k^q are the extended Stevens spin operators.¹⁸ The first term represents the electronic Zeeman interaction and the second term is the effective FS Hamiltonian, describing the interaction of the crystal field with the paramagnetic ion. The order k in the spin operators is restricted by $k \leq 2S$ and $q \leq k$. The last term is due to the manganese hyperfine interaction with $I^{\text{Mn}} = \frac{5}{2}$ for the ${}^{55}\text{Mn}$ isotope with 100% natural abundance.

By exploiting the spin Hamiltonian (1), the obtained experimental spectra can be numerically simulated¹⁹ in order to refine the determined spin-Hamiltonian parameters.

IV. RESULTS AND DISCUSSION

A. Defect structure

In order to systematically study the role of the manganese functional centers in BSPT, several compositions ranging from pure 0.5 mol % Mn-modified PbTiO_3 (Mn:BSPT 0/100) to Mn:BSPT 40/60, including Mn:BSPT 36/64 at the morphotropic phase boundary, have been studied. However, only for the pure-phase Mn:PbTiO₃ composition EPR resonances are observed. The corresponding X-band EPR spectrum is shown in Fig. 1(a), revealing a tetravalent Mn^{4+} oxidation state with $g_{\parallel} = 1.982$, $g_{\perp} = 1.987$, and $|a_{\text{iso}}| = 212$ MHz.^{20,21} A numerically simulated spectrum invoking these spin-Hamiltonian parameters together with $B_2^0 = 3$ GHz and $B_2^2 = 0$ is plotted below the experimental spectrum. Whereas the g values and the ${}^{55}\text{Mn}$ hyperfine splitting can be accurately determined, the fine-structure interaction parameter B_2^0 can only be estimated at X-band frequencies (9.4 GHz).

Correspondingly, the manganese isovalently substitutes at the perovskite B site ($\text{Mn}_{\text{Ti}}^{\times}$),

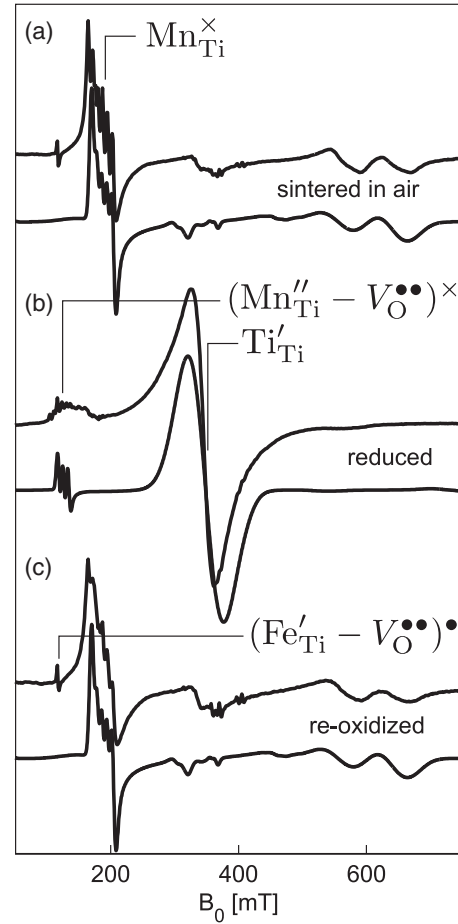


FIG. 1. X-band (9.4 GHz) EPR spectra of 0.5 mol% manganese-modified PbTiO_3 for different heat treatments under varying oxygen partial pressure. (a) Sintered under air. (b) Reduced under H_2 (99.95%). (c) Reoxidized under O_2 (99.8%). Experimental spectra (top) and numerically simulated spectra (bottom).

No signature from magnetically active secondary phases has been observed, indicating that the here used amount of 0.5 mol % manganese is below the solubility limit in lead titanate.^{22,23}

For all compositions containing BiScO_3 , no EPR at X band was observed. Tentatively, all manganese ions may then be incorporated as trivalent manganese according to the following incorporation reactions that account for an incorporation at the Ti or the Sc site:



Trivalent manganese is a so-termed “non-Kramers” ion that is often called being “EPR silent” in the “low-frequency regime” ($|B_2^0| \gg \hbar\omega_{\text{mw}}$).^{24–27} The absence of an EPR signal can be explained by two arguments. First, owing to Mn^{3+} having an *integer* spin state ($S = 2$) with a singlet lying lowest, and second, due to a pronounced orientation dependence of the EPR transitions. Because of the comparatively small microwave quantum of energy in the X band, and owing to the EPR selection rule ($\Delta m_S = \pm 1$) “allowed” EPR transitions either cannot be induced or are largely orientation dependent

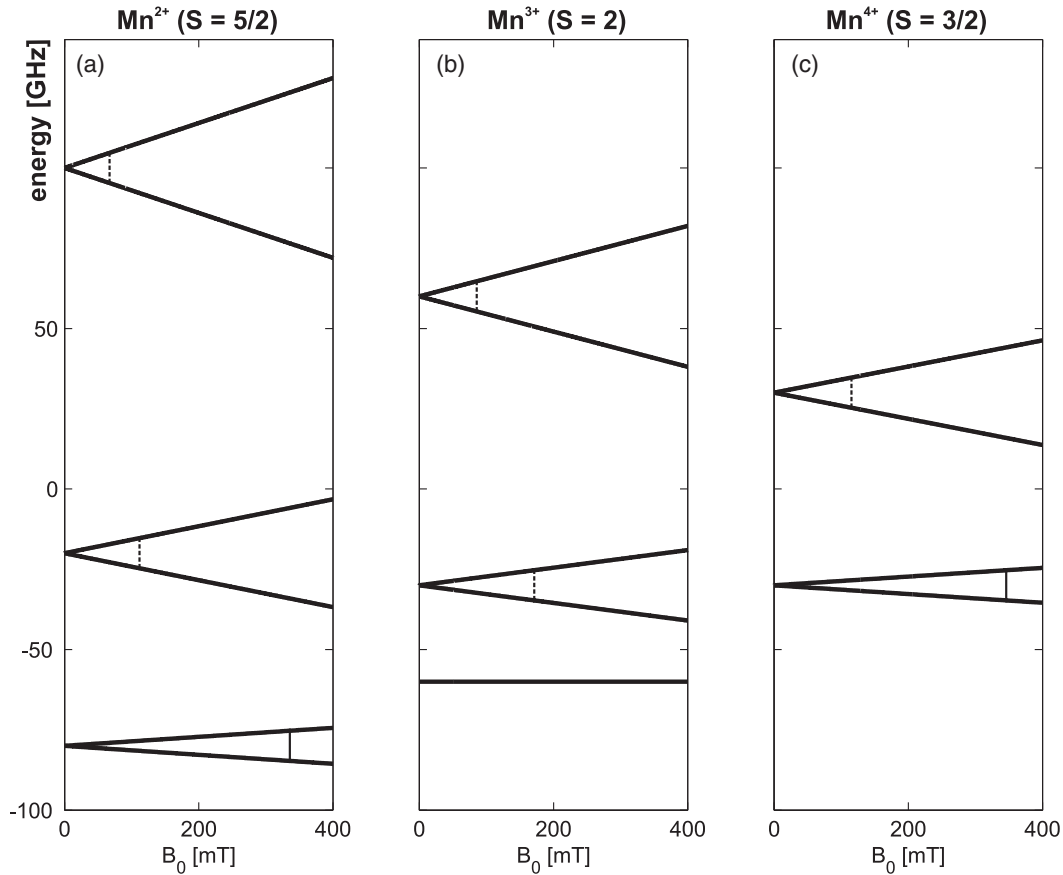


FIG. 2. Schematic representation of the energy levels for manganese-doped BSPT at X band (9.4 GHz). The energy levels are plotted as a function of the magnetic field for the canonical parallel orientations relative to the fine-structure tensor principal axes. B_2^0 is taken to be positive. The EPR transitions for the X-band frequencies are marked by vertical lines involving “allowed” ($\Delta m_S = \pm 1$; solid) and “forbidden” transitions ($\Delta m_S = \pm 2, 3, 4, \dots$; dashed). (a) Mn^{2+} ($3d^5$, $S = \frac{5}{2}$). (b) Mn^{3+} ($3d^4$, $S = 2$). (c) Mn^{4+} ($3d^3$, $S = \frac{3}{2}$).

where fine-structure strain broadens the resonance lines beyond detectability. Consequently, EPR will only be observed for high Larmor frequencies ($|B_2^0| \ll \hbar\omega_{\text{mw}}$) that allow for a mixing of states.^{27,28} This difference between integer and half-integer high-spin states is schematically illustrated in Fig. 2 by means of the corresponding energy-level schemes.

Figures 2(a) and 2(c) are representative for the situations with *half-integer* spin states Mn^{4+} ($S = \frac{3}{2}$) and Mn^{2+} ($S = \frac{5}{2}$). The corresponding energy levels are pairwise degenerate at zero field (“Kramers doublets”) and their degeneracy is lifted by the magnetic field such that even at low Larmor frequencies ($|B_2^0| \gg \hbar\omega_{\text{mw}}$) a central transition with “allowed” EPR transitions $|m_S = -\frac{1}{2}\rangle \rightarrow |+\frac{1}{2}\rangle$ may be induced.

In order to verify the assumption that Mn^{3+} is the present charge state, EPR at high Larmor frequencies ($|B_2^0| \ll \hbar\omega_{\text{mw}}$) in the so-called “high-field regime” has been performed in order to overcome large energy splittings and to reduce second-order effects on the orientation dependence of resonances. The corresponding spectra at 104 GHz and 208 GHz for $[\text{Pb}_{0.64}\text{Bi}_{0.36}][\text{Ti}_{0.64-0.0032}\text{Sc}_{0.36-0.0018}\text{Mn}_{0.005}]\text{O}_3$ (sample C) are depicted in Fig. 3.

The high-field spectra are dominated by a resonance at $g = 1.971$, which is characteristic for the Mn^{3+} state ($3d^4$) with a less than half-filled outer electron shell.^{18,28,29} Although

an anisotropic g matrix typically is observed for Ti^{3+} , only the $g_{xx,yy}$ region has been observed here, such that the g_{zz} region is expected to be broadened beyond detectability. Additionally, as compared to the spectrum for the Mn^{4+} state, no resolved ^{55}Mn hyperfine pattern is observed due to powder averaging of the comparatively strong angular-dependent EPR transitions. Whereas for Mn^{2+} and Mn^{4+} the central transition ($|m_S = -\frac{1}{2}\rangle \rightarrow |+\frac{1}{2}\rangle$) shows a relatively small orientation dependence ($\delta B_0^{\text{Mn}^{2,4+}} \approx 0.003$ T), in the case of Mn^{3+} a much more pronounced orientation dependence occurs for the observed $|m_S = \pm 1\rangle \rightarrow |0\rangle$ transitions ($\delta B_0^{\text{Mn}^{3+}} \approx 0.1$ T). This situation is schematically illustrated in Fig. 4 for a Larmor frequency of 104 GHz.

Higher transitions are not observed in the EPR spectra owing to extensive fine-structure strain, for which reason the corresponding transitions are broadened such that they cannot be detected with the experimental modulation amplitude available.

Concerning the site of incorporation, based on the EPR results only, it is not possible to distinguish whether the Mn^{3+} centers substitute for titanium or scandium. In the case of a substitution for Ti^{4+} according to Eq. (3), it would result in an acceptor-type center ($\text{Mn}_{\text{Ti}}^{3+}$) rendering a “hard” material, whereas the incorporation at a Sc^{3+} site according

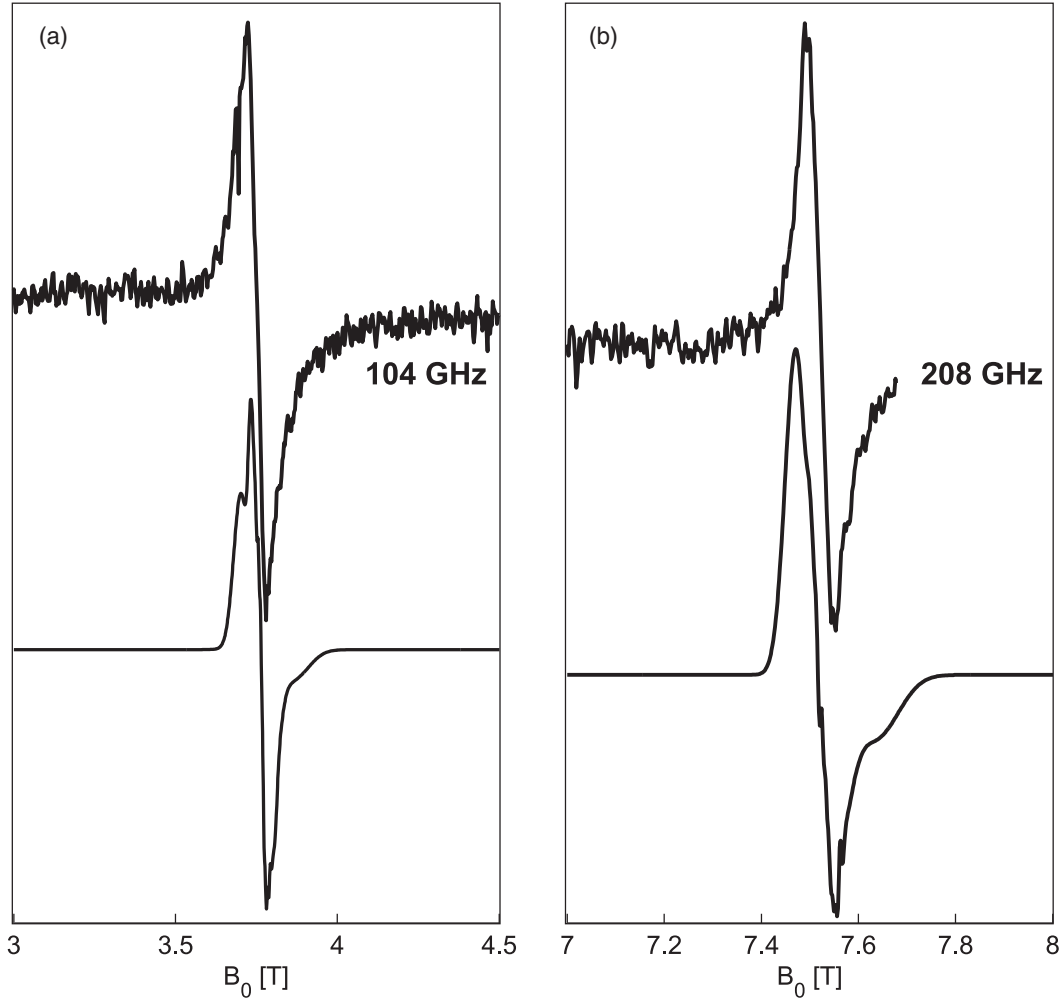


FIG. 3. High-frequency EPR-spectra of 0.5 mol% manganese-doped BSPT ($[\text{Pb}_{0.64}\text{Bi}_{0.36}][\text{Ti}_{0.64-0.0032}\text{Sc}_{0.36-0.0018}\text{Mn}_{0.005}]\text{O}_3$, sample C) at Larmor frequencies of 104 GHz (a) and 208 GHz (b). Experimental spectra (top) and numerically simulated spectra (bottom).

to Eq. (4) would result in an isovalent center ($\text{Mn}_{\text{Sc}}^{\times}$). We thus monitored the corresponding P - E hysteresis loops of the manganese-modified BSPT compounds with respect to a possible “hardening” effect (see Fig. 5).

B. Ferroelectric properties

The corresponding $P(E)$ and $S(E)$ hysteresis loops for undoped and Mn-substituted BSPT 36/64 are shown in Fig. 5. Undoped BSPT 36/64 (sample A) and three compounds with varying Sc/Ti stoichiometry were investigated, namely $[\text{Pb}_{0.64}\text{Bi}_{0.36}][\text{Ti}_{0.64}\text{Sc}_{0.36-0.005}\text{Mn}_{0.005}]\text{O}_3$ (sample B), $[\text{Pb}_{0.64}\text{Bi}_{0.36}][\text{Ti}_{0.64-0.0032}\text{Sc}_{0.36-0.0018}\text{Mn}_{0.005}]\text{O}_3$ (sample C), and $[\text{Pb}_{0.64}\text{Bi}_{0.36}][\text{Ti}_{0.64-0.005}\text{Sc}_{0.36}\text{Mn}_{0.005}]\text{O}_3$ (sample D). These account for a nominal incorporation of the manganese on the Sc site (Mn_{Sc}), the Ti site (Mn_{Ti}), and a mixed incorporation on both B sites ($\text{Mn}_{\text{Sc,Ti}}$), respectively.

Obviously, upon manganese-substitution remanent polarization (P_r) and peak-to-peak strain (S_{pp}) are significantly reduced, whereas the coercive field (E_c) almost remains constant. An evaluation of frequency-dependent strain measurements indicates slightly higher E_c for samples C and D as compared to sample B, which at maximum could be due

to a marginal *hardening* of the material. However, these small changes are not significant and alternatively could also be induced by a distortion of the perovskite structure owing to lattice defects originating from the material’s nonstoichiometry that results if the manganese is preferentially incorporated on the Sc sites.

The large difference in remanent polarization and peak-to-peak strain for undoped as compared to Mn-substituted BSPT is due to microstructural differences, such as variations in grain size as a function of Mn substitution (see Table I). The apparently reduced polarization and total strain is well correlated with the recently reported weakened piezoelectric parameter (d_{33}).⁹

Correspondingly, there is no observable indication of materials *hardening*. This assignment is further supported by the observation that the $P(E)$ hysteresis loop is not “pinched,” which generally is an indication of materials hardening. As a consequence, the manganese ions are isovalently incorporated into the lattice ($\text{Mn}_{\text{Sc}}^{\times}$) on a scandium site as described in Eq. (4). A simple consideration of the corresponding sizes of ionic radii for sixfold coordination,³⁴ with $r_{\text{Sc}^{3+}} = 73$ pm and $r_{\text{Ti}^{4+}} = 68$ pm, as compared to $r_{\text{Mn}^{3+}} = 78.5$ pm and $r_{\text{Mn}^{4+}} = 67$ pm, supports this assignment.

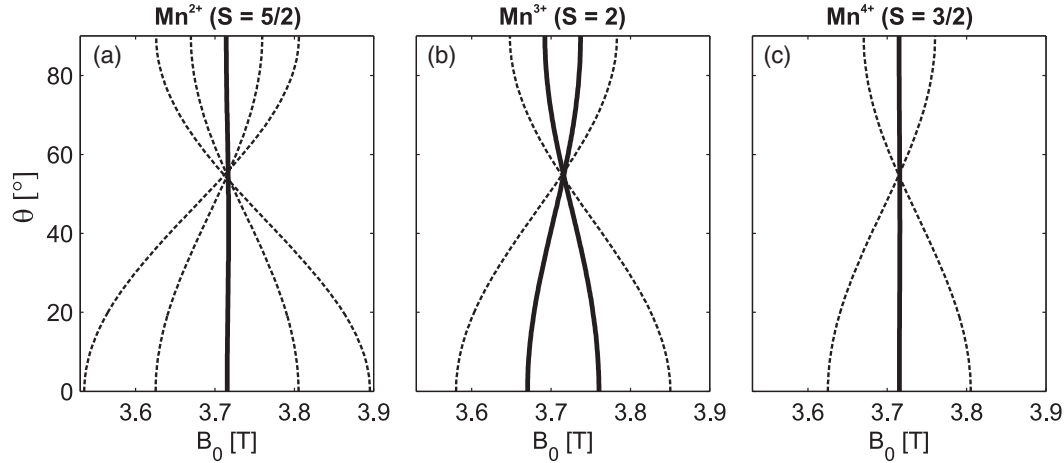


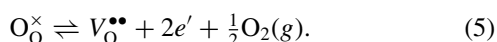
FIG. 4. Orientation dependence of the EPR transitions for manganese-doped BSPT at W band (104 GHz). (a) Mn^{2+} ($S = \frac{5}{2}$). (b) Mn^{3+} ($S = 2$). (c) Mn^{4+} ($S = \frac{3}{2}$). For the half-integer spin-systems Mn^{2+} and Mn^{4+} , the “central transition” $|m_S = -\frac{1}{2}\rangle \rightarrow |+\frac{1}{2}\rangle$ and for the integer spin-system Mn^{3+} the transitions $|m_S = \pm 1\rangle \rightarrow |0\rangle$ are plotted bold. The higher transitions are plotted dashed.

This also involves the formation of an increased amount of additional lattice defects for samples C and D, because the stoichiometry was calculated for manganese incorporated (partly) on the titanium site, but effectively it substitutes for the scandium site.

C. Conductivity mechanism

These additionally formed lattice defects in turn have a pronounced effect on the temperature-dependent DC conductivity, as shown in Fig. 6. Obviously, the manganese-substitution considerably enhances the electrical resistivity. Furthermore, sample B has about two orders of magnitude gain in resistivity, whereas samples C and D for which additional defects are expected have resistivities in between the range spanned by samples A and B. This observation can be explained by assuming the additional lattice defects contributing to the conductivity in the BSPT compounds. Because no further EPR resonances were observed for varying materials’ nonstoichiometry, paramagnetic lattice defects, such as singly ionized V_O^\bullet or polaronic Ti'_{Ti} states, can be ruled out. The additionally formed lattice defects have thus to be diamagnetic and include unbound $V_O^{\bullet\bullet}$ that may contribute to the conductivity via a drift-diffusion mechanism.³⁵ This assignment is supported by the determined transport activation energies (see Table I) that are in the range reported for ionic transport in ferroelectrics³⁶ but exceed the activation energy for electronic transport by one order of magnitude.

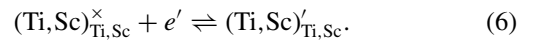
To study the interplay between the manganese functional centers with the mechanism of electrical conductivity in more detail, heat-treated samples under varying oxygen partial pressure were analyzed by EPR. The effect of reducing conditions on the defect structure may be described on an atomic level as follows: Owing to the low oxygen partial pressure, the oxygen is exchanged between the solid BSPT and the surrounding atmosphere according to the reaction³⁰



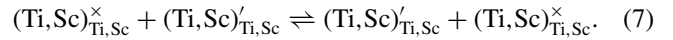
The electrons generated in this reaction are first associated with the oxygen vacancies (V_O^\times), which in turn are subsequently

rapidly thermally ionized ($V_O^{\bullet\bullet}$) owing to the proximity of these levels to the conduction band edge.

For an undoped BSPT material, these electrons may be trapped by the B-site ions according to the following conduction mechanisms, depending on either of the two different B-site ions (Ti, Sc). The corresponding trapping mechanism is described by means of the following set of equations:



Hereby, the electrons are typically almost fully delocalized on the titanium and possibly also on the scandium ions according to the following equilibrium:³¹



If the role of the $\text{Mn}_{\text{Sc}}^\times$ consists in trapping conduction electrons (e') a change in valence state ($\text{Mn}_{\text{Sc}}^\times \rightarrow \text{Mn}'_{\text{Sc}}$) should be observed by EPR. As this involves the change from a half-integer to an integer electron spin state, and vice versa, at X-band an “EPR-visible” state may be turned into an “EPR-silent” state. If on the other hand, the $\text{Mn}_{\text{Sc}}^\times$ trap an oxygen vacancy ($V_O^{\bullet\bullet}$) by forming a defect complex similar to ferroelectric BaTiO_3 ,^{32,33} the corresponding variation in electric field gradient will be monitored via an increase in the electron fine-structure interaction.

1. Mn-modified PbTiO_3

Starting with the pure-member phase Mn:PbTiO_3 , after the reduction treatment the $\text{Mn}_{\text{Ti}}^\times$ signal in PbTiO_3 disappeared, as shown in Fig. 1. This corresponds to the formation of acceptor-type Mn'_{Ti} centers. Additionally, an intensive resonance at $g = 1.931$ occurs that has not been observed in the sample sintered under air. Because of any absent hyperfine structure and owing to $g < g_e = 2.0023$, the free-electron g value, which is characteristic for ions with a less than half-filled shell, this signal is attributed to Ti'_{Ti} acceptor centers.^{37–42} Although this g value is close to the one determined for the $\text{Mn}_{\text{Sc}}^\times$ center in BSPT 36/64 ($g = 1.971$), we assign this resonance rather to Ti'_{Ti} -acceptor states ($3d^1$, $S = \frac{1}{2}$) because the integer high-spin

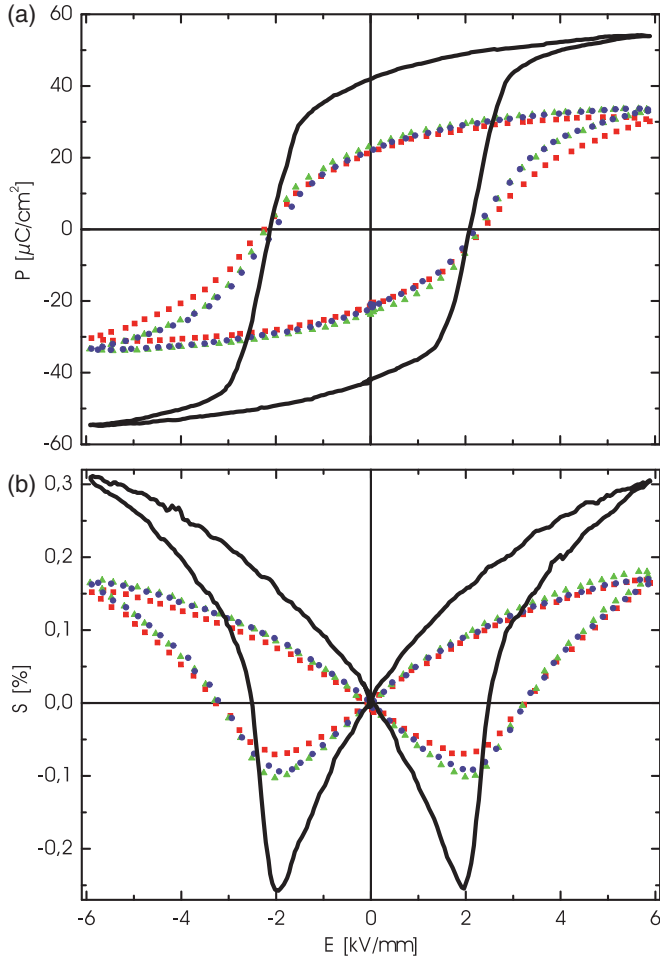


FIG. 5. (Color online) Polarization (a) and strain (b) hysteresis loops of bipolar loading of Mn-substituted BSPT 36/64 measured at 100 mHz. Undoped BSPT 36/64 (solid black line), $[\text{Pb}_{0.64}\text{Bi}_{0.36}][\text{Ti}_{0.64}\text{Sc}_{0.36-0.005}\text{Mn}_{0.005}]\text{O}_3$ (red circle), $[\text{Pb}_{0.64}\text{Bi}_{0.36}][\text{Ti}_{0.64-0.0032}\text{Sc}_{0.36-0.0018}\text{Mn}_{0.005}]\text{O}_3$ (green triangle), and $[\text{Bi}_{0.36}\text{Pb}_{0.64}][\text{Sc}_{0.36}\text{Ti}_{0.64-0.005}\text{Mn}_{0.005}]\text{O}_3$ (blue rhomb).

Mn^{3+} state ($3d^4$, $S = 2$) is not observable at the low-frequency condition used here.

Furthermore, a less intense signal at 180 mT is observed. Because of the characteristic sextet ^{55}Mn hyperfine structure owing to the interaction with the 100% abundant nucleus with $I = \frac{5}{2}$, this signal is assigned to manganese in the low-field regime ($B_2^0 \gg \hbar\omega_{\text{mw}}$). The strong fine-structure interaction is sensitive to the formation of $(\text{Mn}_{\text{Ti}}'' - \text{V}_{\text{O}}^{\bullet\bullet})^\times$ defect complexes. Consequently, the Mn_{Ti}'' centers act as trapping centers for oxygen vacancies and thus reduce the ionic mobility in lead titanate. Owing to the the small concentration of the $(\text{Mn}_{\text{Ti}}'' - \text{V}_{\text{O}}^{\bullet\bullet})^\times$ center in the reduced specimen, a considerable amount of EPR-silent Mn_{Ti}' centers is expected for this compound. Because acceptor-type functional centers typically form defect complexes with charge-compensating oxygen vacancies,⁴³⁻⁴⁷ these are expected to exist as $(\text{Mn}_{\text{Ti}}' - \text{V}_{\text{O}}^{\bullet\bullet})^\bullet$ defect complexes.

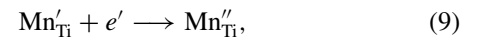
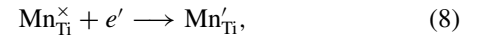
Furthermore, for the PbTiO_3 compound, in addition to the manganese resonances an impurity signal from $(\text{Fe}_{\text{Ti}}' - \text{V}_{\text{O}}^{\bullet\bullet})^\bullet$ defect complexes occurs.^{48,49} However, its intensity is not

TABLE I. Materials properties for the different ceramic undoped and manganese-substituted BSPT 36/64 samples. Undoped BSPT 36/64 (A), $[\text{Pb}_{0.64}\text{Bi}_{0.36}][\text{Ti}_{0.64}\text{Sc}_{0.36-0.005}\text{Mn}_{0.005}]\text{O}_3$ (B), $[\text{Pb}_{0.64}\text{Bi}_{0.36}][\text{Ti}_{0.64-0.0032}\text{Sc}_{0.36-0.0018}\text{Mn}_{0.005}]\text{O}_3$ (C), and $[\text{Bi}_{0.36}\text{Pb}_{0.64}][\text{Sc}_{0.36}\text{Ti}_{0.64-0.005}\text{Mn}_{0.005}]\text{O}_3$ (D).

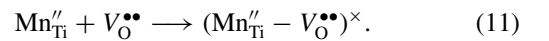
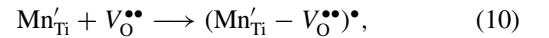
	Sample A	Sample B	Sample C	Sample D
Grain size (μm)	1.3	8.9	13.4	16.4
P_r ($\mu\text{C}/\text{cm}^2$)	42	21	23	22
S_{pp} (%)	0.56	0.24	0.28	0.26
E_a (eV)		1.62	1.74	1.82

affected by the reduction treatment, indicating that neither e' nor $\text{V}_{\text{O}}^{\bullet\bullet}$ may be trapped at the $(\text{Fe}_{\text{Ti}}' - \text{V}_{\text{O}}^{\bullet\bullet})^\bullet$ site.

The overall charge compensation for manganese-modified PbTiO_3 thus involves valency-altered Ti_{Ti}' and Mn_{Ti}' , as well as $(\text{Mn}_{\text{Ti}}' - \text{V}_{\text{O}}^{\bullet\bullet})^\bullet$ and $(\text{Mn}_{\text{Ti}}' - \text{V}_{\text{O}}^{\bullet\bullet})^\times$ defect complexes. Correspondingly, the enhanced resistivity is owing to the trapping of electronic charge carriers via Eq. (6) and the reduction of the manganese functional centers according to



as well as the trapping of ionic charge carriers and the formation of defect complexes according to



Concerning the condition for charge neutrality, the defect equilibrium has the following form:

$$2[\text{V}_{\text{Pb}}''] + [\text{Ti}_{\text{Ti}}'] + [\text{Mn}_{\text{Ti}}'] \approx [(\text{Mn}_{\text{Ti}}' - \text{V}_{\text{O}}^{\bullet\bullet})^\bullet] + 2[\text{V}_{\text{O}}^{\bullet\bullet}]. \quad (12)$$

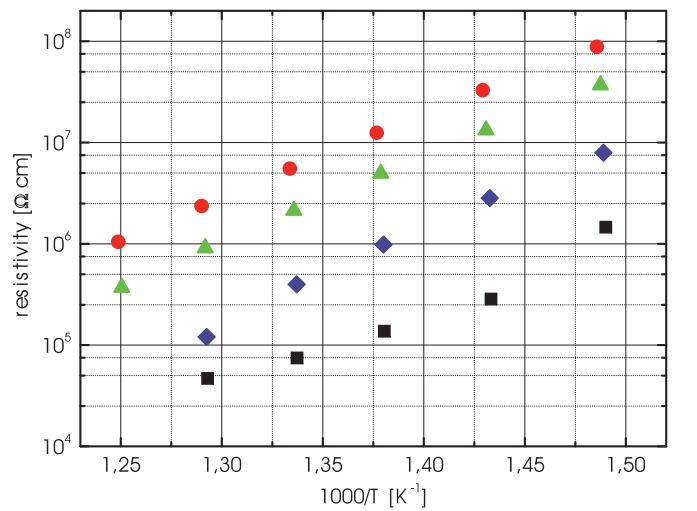


FIG. 6. (Color online) Temperature-dependent DC conductivity at 200 V mm between 250 °C and 500 °C for undoped and manganese-substituted BSPT 36/64. Undoped BSPT 36/64 (black square), $[\text{Pb}_{0.64}\text{Bi}_{0.36}][\text{Ti}_{0.64}\text{Sc}_{0.36-0.005}\text{Mn}_{0.005}]\text{O}_3$ (red circle), $[\text{Pb}_{0.64}\text{Bi}_{0.36}][\text{Ti}_{0.64-0.0032}\text{Sc}_{0.36-0.0018}\text{Mn}_{0.005}]\text{O}_3$ (green triangle), and $[\text{Bi}_{0.36}\text{Pb}_{0.64}][\text{Sc}_{0.36}\text{Ti}_{0.64-0.005}\text{Mn}_{0.005}]\text{O}_3$ (blue rhomb).

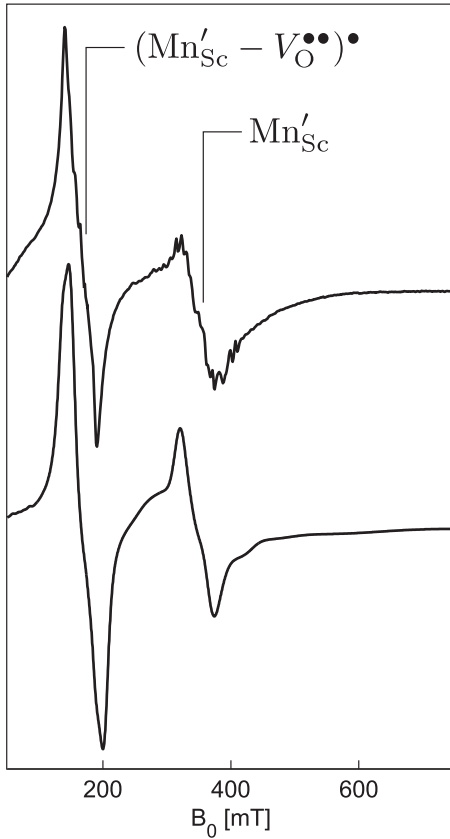
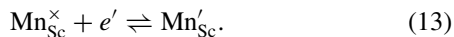


FIG. 7. X-band (9.4 GHz) EPR spectra of 0.5 mol% manganese-modified BSPT 36/64 after reducing heat treatment under H_2 (99.95%). Experimental spectrum (top) and numerically simulated spectrum (bottom).

Because the $(\text{Mn}'_{\text{Ti}} - \text{V}_\text{O}^{\bullet\bullet})^\bullet$ defect complex electrically acts as a donor, part of the acceptor-type Mn'_{Ti} centers are self-compensated.

2. Mn-modified BSPT 36/64

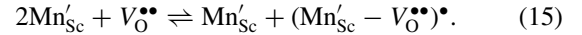
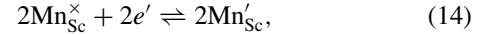
With respect to the solid-solution system Mn:BSPT 36/64, the initially EPR-silent $\text{Mn}^\times_{\text{Sc}}$ center is transformed after reduction into an EPR spectrum with two resonances at 180 mT and 340 mT, as shown in Fig. 7. The latter signal is in agreement with the one for an Mn^{2+} charge state.^{21,50-53} Contrary to the situation for PbTiO_3 , the $\text{Mn}^\times_{\text{Sc}}$ provides a deeper trap for electrons than $\text{Ti}^\times_{\text{Ti}}$. Consequently, a change in valency $\text{Mn}^\times_{\text{Sc}} \rightarrow \text{Mn}'_{\text{Sc}}$ is observed after the reduction treatment; owing to the trapping of an electron at the $\text{Mn}^\times_{\text{Sc}}$ site, the electrons are preferentially trapped on these sites, replacing Eq. (6):



In analogy to the “pure” phase Mn:PbTiO_3 , also an oxygen vacancy is trapped at the valency-altered Mn'_{Sc} centers.

However, in the case of Mn:BSPT the defect-complex signal is considerably more intense as compared to lead titanate. The explanation of this observation may be twofold: Either the trapping of $\text{V}_\text{O}^{\bullet\bullet}$ in BSPT is more efficient than in PT, or the ionic conduction by means of $\text{V}_\text{O}^{\bullet\bullet}$ migration plays a considerably more pronounced role in BSPT than in PT.

The resulting mechanism for trapping electronic and ionic charges in Mn:BSPT is thus according to



Concerning the overall charge compensation, for manganese-modified BSPT Mn'_{Sc} and $(\text{Mn}'_{\text{Sc}} - \text{V}_\text{O}^{\bullet\bullet})^\bullet$ have been observed by EPR. The two kinds of defects mutually compensate, such that the following defect equilibrium,

$$[\text{Mn}'_{\text{Sc}}] \approx [(\text{Mn}'_{\text{Sc}} - \text{V}_\text{O}^{\bullet\bullet})^\bullet], \quad (16)$$

is present.

Finally, the observed manganese valency changes are completely reversible after an oxidation treatment for all PT (see Fig. 1) and BSPT compounds (not shown).

The mechanisms for enhanced electrical resistivity in manganese-substituted BSPT compounds reported here thus support the existence of similar mechanisms that have been previously proposed for the manganese impurity centers in BaTiO_3 .⁵⁴

V. CONCLUSION AND OUTLOOK

In conclusion, the effect of multivalency manganese doping on the defect structure has been studied, explaining the mechanism for enhanced electrical resistivity for the high-temperature piezoelectric $(1-x)\text{BiScO}_3-x\text{PbTiO}_3$. The results show that manganese is incorporated on a scandium rather than a titanium site as an isovalent substitute ($\text{Mn}^\times_{\text{Sc}}$) instead of an acceptor-type center, such as Mn'_{Ti} , Mn''_{Ti} , or Mn'_{Sc} . The enhanced electric resistivity is found being on the one hand due to the trapping of conduction electrons at the manganese functional center sites ($\text{Mn}^\times_{\text{Sc}} + e' \rightarrow \text{Mn}'_{\text{Sc}}$). On the other hand, through the formation of $(\text{Mn}'_{\text{Sc}} - \text{V}_\text{O}^{\bullet\bullet})^\bullet$ defect complexes the ionic conductivity is reduced. Concerning the overall mechanism of charge compensation in that material, both kinds of defects mutually compensate.

ACKNOWLEDGMENTS

This research was partly supported by the Deutsche Forschungsgemeinschaft and EuroMagNET (EU Contract No. 228043), as well as the DFG Center of Excellence 595 “Electrical Fatigue in Functional Materials.” Many helpful discussions with Prof. Jürgen Rödel (TU Darmstadt) and Prof. Donald M. Smyth (Lehigh) are gratefully acknowledged.

*Corresponding author: r.eichel@physchem.uni-freiburg.de

¹D. Damjanovic, *Curr. Opin. Solid State Mater. Sci.* **3**, 469 (1998).

²R. E. Eitel, C. A. Randall, T. R. Shrout, and S. E. Park, *Jpn. J. Appl. Phys.* **41**, 2099 (2002).

³R. E. Eitel, S. J. Zhang, T. R. Shrout, C. A. Randall, and I. Levin, *J. Appl. Phys.* **96**, 2828 (2004).

⁴R. C. Turner, P. A. Fugier, R. E. Newnham, and T. R. Shrout, *Appl. Acoust.* **41**, 299 (1994).

- ⁵C. A. Randall, R. E. Eitel, T. R. Shrout, D. I. Woodward, and I. M. Reaney, *J. Appl. Phys.* **93**, 9271 (2003).
- ⁶Y. Shimojo, R. Wang, T. Sekiya, T. Nakamura, and L. E. Cross, *Ferroelectrics* **284**, 121 (2003).
- ⁷S. Chen, X. L. Dong, C. L. Mao, and F. Cao, *J. Am. Ceram. Soc.* **89**, 3270 (2006).
- ⁸T. Zou, X. Wang, H. Wang, C. Zhong, L. Li, and I. W. Chen, *Appl. Phys. Lett.* **93**, 192913 (2008).
- ⁹S. J. Zhang, R. E. Eitel, C. A. Randall, T. R. Shrout, and E. F. Alberta, *Appl. Phys. Lett.* **86**, 262904 (2005).
- ¹⁰D. Damjanovic, *Rep. Prog. Phys.* **61**, 1267 (1998).
- ¹¹S. J. Zhang, N. Kim, T. R. Shrout, M. Kimura, and A. Ando, *Solid State Commun.* **140**, 154 (2006).
- ¹²X. L. Liu, Z. Xu, S. B. Qu, X. Y. Wei, and J. L. Chen, *Ceram. Int.* **34**, 797 (2008).
- ¹³A. B. Kounga Njiwa, E. Aulbach, J. Rödel, S. L. Turner, T. P. Comyn, and A. J. Bell, *J. Am. Ceram. Soc.* **89**, 1761 (2006).
- ¹⁴R.-A. Eichel, *J. Am. Ceram. Soc.* **91**, 691 (2008).
- ¹⁵R.-A. Eichel, *Phys. Chem. Chem. Phys.* **13**, 368 (2011).
- ¹⁶R.-A. Eichel and H. Kungl, *Funct. Mater. Lett.* **3**, 1 (2010).
- ¹⁷S. A. Zvyagin, J. Krzystek, P. H. M. van Loosdrecht, G. Dhalenne, and A. Revcolevschi, *Physica B* **346–347**, 1 (2004).
- ¹⁸A. Abragam and B. Bleaney, *Electron Paramagnetic Resonance of Transition Ions* (Clarendon Press, Oxford, 1970).
- ¹⁹S. Stoll and A. Schweiger, *J. Magn. Reson.* **178**, 42 (2006).
- ²⁰E. Erdem, M. D. Drahus, R.-A. Eichel, A. Ozarowski, J. van Tol, and L. C. Brunel, *Ferroelectrics* **363**, 39 (2008).
- ²¹G. Klotzsche, W. Windsch, and K. Wojcik, *Ferroelectrics Lett.* **15**, 115 (1993).
- ²²H.-J. Kleebe, S. Lauterbach, L. Silvestroni, H. Kungl, M. J. Hoffmann, E. Erdem, and R.-A. Eichel, *Appl. Phys. Lett.* **94**, 142901 (2009).
- ²³E. Aksel, E. Erdem, P. Jakes, J. L. Jones, and R.-A. Eichel, *Appl. Phys. Lett.* **97**, 012903 (2010).
- ²⁴D. P. Goldberg, J. Telser, J. Krzystek, A. G. Montalban, L. C. Brunel, A. G. M. Barrett, and B. M. Hoffman, *J. Am. Chem. Soc.* **119**, 8722 (1997).
- ²⁵J. D. Harvey, C. J. Ziegler, J. Telser, A. Ozarowski, and J. Krzystek, *Inorg. Chem.* **44**, 4451 (2005).
- ²⁶M. D. Drahus, P. Jakes, E. Erdem, and R.-A. Eichel, *Solid State Ionics* **184**, 47 (2011).
- ²⁷E. Aksel, P. Jakes, E. Erdem, D. M. Smyth, A. Ozarowski, J. van Tol, J. L. Jones, and R.-A. Eichel, *J. Am. Ceram. Soc.* **94**, 1363 (2011).
- ²⁸J. Krzystek, A. Ozarowski, and J. Telser, *Coord. Chem. Rev.* **250**, 2308 (2006).
- ²⁹R.-A. Eichel, *J. Electroceram.* **19**, 9 (2007).
- ³⁰F. Batllo, E. Duverger, J. Jules, J. Niepce, B. Jannot, and M. Maglione, *Ferroelectrics* **109**, 113 (1990).
- ³¹H. Ihrig and D. Hennings, *Phys. Rev. B* **17**, 4593 (1978).
- ³²R.-A. Eichel and R. Böttcher, *Mol. Phys.* **105**, 2195 (2007).
- ³³L. X. Zhang, E. Erdem, X. Ren, and R.-A. Eichel, *Appl. Phys. Lett.* **93**, 202901 (2008).
- ³⁴R. D. Shannon, *Acta Crystallogr. Sect. A* **32**, 751 (1976).
- ³⁵Y. A. Genenko, *Phys. Rev. B* **78**, 214103 (2008).
- ³⁶D. M. Smyth, *Ferroelectrics* **151**, 115 (1994).
- ³⁷R. Scharfschwerdt, A. Mazur, O. F. Schirmer, H. Hesse, and S. Mendricks, *Phys. Rev. B* **54**, 15284 (1996).
- ³⁸S. Lenjer, O. F. Schirmer, H. Hesse, and T. W. Kool, *Phys. Rev. B* **66**, 165106 (2002).
- ³⁹V. V. Laguta, M. D. Glinchuk, I. P. Bykov, Y. L. Maksimenko, J. Rosa, and L. Jastrabik, *Phys. Rev. B* **54**, 12353 (1996).
- ⁴⁰T. Kolodiaznyi and A. Petric, *J. Phys. Chem. Solids* **64**, 953 (2003).
- ⁴¹T. Kolodiaznyi, A. Younker, P. Malysz, and P. Mascher, *Mater. Sci. Forum* **445–446**, 129 (2004).
- ⁴²E. Erdem, P. Jakes, R.-A. Eichel, D. C. Sinclair, M. Pasha, and I. M. Reaney, *Funct. Mater. Lett.* **3**, 65 (2010).
- ⁴³E. Siegel and K. A. Müller, *Phys. Rev. B* **19**, 109 (1979).
- ⁴⁴W. L. Warren, B. A. Tuttle, F. C. Rong, G. J. Gerardi, and E. H. Poindexter, *J. Am. Ceram. Soc.* **80**, 680 (1997).
- ⁴⁵H. Meštrić, R.-A. Eichel, T. Kloss, K.-P. Dinse, So. Laubach, St. Laubach, P. C. Schmidt, K. A. Schönau, M. Knapp, and H. Ehrenberg, *Phys. Rev. B* **71**, 134109 (2005).
- ⁴⁶R.-A. Eichel, P. Erhart, P. Träskelin, K. Albe, H. Kungl, and M. J. Hoffmann, *Phys. Rev. Lett.* **100**, 095504 (2008).
- ⁴⁷R.-A. Eichel, E. Erüna, M. D. Drahus, D. M. Smyth, J. van Tol, J. Acker, H. Kungl, and M. J. Hoffmann, *Phys. Chem. Chem. Phys.* **11**, 8698 (2009).
- ⁴⁸E. Erdem, R.-A. Eichel, H. Kungl, M. J. Hoffmann, A. Ozarowski, J. van Tol, and L. C. Brunel, *Phys. Scr.*, **T 129**, 12 (2007).
- ⁴⁹P. Jakes, E. Erdem, R.-A. Eichel, L. Jin, and D. Damjanovic, *Appl. Phys. Lett.* **98**, 072907 (2011).
- ⁵⁰H. Ikushima and S. Hayakawa, *J. Phys. Soc. Jpn.* **27**, 414 (1969).
- ⁵¹D. Hennings and H. Pomplun, *J. Am. Ceram. Soc.* **57**, 527 (1974).
- ⁵²D. Hennings, *Jpn. J. Appl. Phys.* **37**, 5237 (1998).
- ⁵³A. Molak and K. Wojcik, *Ferroelectrics* **125**, 349 (1992).
- ⁵⁴S. Jida and T. Miki, *J. Appl. Phys.* **80**, 5234 (1996).